Luetzow, K., Weigel, T. & Lendlein, A.:
Solvent-based Fabrication Method for Magnetic, Shape-Memory Nanocomposite Foams.
In: MRS Advances 5, 785–795 (2020).
First published online by Cambridge University Press: 15.11.2019

https://doi.org/10.1557/adv.2019.422

Solvent-based Fabrication Method for Magnetic, Shape-Memory Nanocomposite Foams

Karola Luetzow[1], Thomas Weigel[1], Andreas Lendlein[1,2]

1 Institute of Biomaterial Science and Berlin-Brandenburg Centre for Regenerative Therapies, Helmholtz-Zentrum Geesthacht, Teltow, Germany;
2 Institute of Chemistry, University of Potsdam, Potsdam, Germany

*Correspondence to: Prof. Andreas Lendlein
andreas.lendlein@hzg.de

Key words: composite, foam, polymer, magnetic, shape memory

ABSTRACT

Shape-memory foams, which can be temporarily fixed in their compressed state and be expanded on demand. Here, highly porous, nanocomposite foams were prepared from a solution of a polyetherurethane with suspended nanoparticles a mean aggregate size of 90 nm (2.5, 5, 10 wt%), which have an iron (III)oxide core of a mean domain size of 20-26 nm covered with a silica shell. The polymer solution with suspended nanoparticles was cooled down to -20 °C in a two-stage process, which was followed by freeze-drying. The average pore size increases with decreasing amount of nanoparticles from 158 µm to 230 µm while the foam porosity remained constant. After fixation of a temporary form of the nanocomposite foams, shape recovery can be triggered either by heat or by exposure to an alternating magnetic field. Compressed foams showed a recovery rate of up to 76 ± 4% in a thermochamber at 80 °C, and a slightly lower recovery rate of up to 65 ± 4% in a magnetic field.

INTRODUCTION:

Devices made from shape-memory polymers (SMP) can be transported or stored efficiently in a smaller shape and then be transformed into their application relevant shape [1-5]. Fibers [6, 7], flat sheets folding [8] up to cubes or compressed foams have been considered as shaped bodies [9]. The stimulus inducing the shape-memory effect (SME) can be heat or light [10-12] or even alternating magnetic fields [5, 6, 13-17]. Initiation of the SME by alternating magnetic fields has been reported for polymeric films with incorporated magnetic particles having diameters in the nano- to micrometer size range [6, 16, 18]. Various ferro- or ferromagnetic cores have been investigated, among them iron (III) oxide particles with a silica matrix embedded in a polymer, e.g. a polyetherurethane (PEU) [6]. PEU is a copolymer consisting of hard segments from bis(*p*-cyclohexyl

isocyanate)(H_{12}MDI)/1,4-butanediol and soft segments from H_{12}MDI /poly(tetramethylene glycol). The SME is based on the glass transition of the switching phase consisting of a mixed phase. This glass transition has a rather broad range from 20 °C to 90 °C [6, 9]. Inductive heating in alternating magnetic-fields is a remote, contact-free stimulation, and can be applied in situations in which a direct heating by a warm fluid or gas is not possible.

SMP foams [19] have been prepared with various methods and are of high interest not only for medical applications [20]. They have been prepared by thermally induced phase separation (TIPS) [9], by processing with supercritical carbon dioxide, by particle leaching [21-24] or during synthesis of a polyurethane using water as a blowing agent [25, 26]. The latter method has been used for the preparation of a SMP composite foam with inorganic particles by incorporating isocyanate-modified silica nanoparticles in the reaction. The incorporation of inorganic particles in SMP foams or porous bodies has been studied i.e. for clay [27], carbon nanotubes [23, 28] or hydroxyapatite [29].

It is hypothesized that highly porous nanocomposite foams consisting of PEU and magnetic nanoparticles can be prepared by TIPS and that the SME of these foams can be triggered in an alternating magnetic field by inductive heating. Fe(III)oxide nanoparticles with a silica matrix were selected, as the silica shell helps to stabilize the nanoparticles and silica is resistant to the organic solvents used for TIPS. A mean aggregate size of 90 nm of an aqueous dispersion and a mean domain size (x-diffraction) of 20-26 nm for these particles has been reported [6]. Foams have been prepared from PEU with the TIPS method and have shown excellent recoveries upon heating [9]. TIPS employs a polymer solution, which is cooled down according to a selected cooling procedure [30-32]. The first challenge of this work was freezing the polymer solution with the suspended nanoparticles before the incorporated nanoparticles would sediment, which would obviously lead to an inhomogeneous distribution, and thus inhomogeneous heating of the foam within the magnetic field. Details on the highly porous morphology of the foams have been investigated by scanning electron microscopy (SEM) and X-ray computed microtomography (μ-CT). A further challenge was to overcome the environmental cooling of the open porous foam during inductive heating which is caused by the high surface to volume ratio. The inductive heating of the foams in a magnetic field to induce the SME will be compared to those by environmental heating of a sample in a tensile tester and a free standing sample.

EXPERIMENTAL DETAILS

Fabrication method for the nanocomposite foams

A solution of the 5 wt% Tecoflex EG 72D (PEU; Noveon Thermedics, Wilmington, MA, USA) in dioxane with a water content of 5% (v/v) was prepared at 80 °C, to which iron (III)oxide nanoparticles covered with silica matrix (adnano Magsilica 50, Degussa, Hanau, Germany) were added (2.5, 5, and 10 wt% yielding the foams C-PEU2.5, C-PEU5, and C-PEU10) under light shaking at 20 °C. The suspension was poured into plastic vials with a diameter of 3.1 cm (20 g suspension per vial) cooled under light shaking to 10 °C and then placed into a cooling chamber at -20 °C for 16 hours to freeze the suspension. The Magsilica nanoparticles have a mean aggregate size of 90 nm (determination by photon correlation spectroscopy of an aqueous dispersion) [6]. The solvent was removed by freeze-drying (ALPHA 2-4 LSC, Martin Christ Gefriertrocknungsanlagen gmbh, Osterode am Harz, Germany). Afterwards the foams were placed into vaccum oven 48 h (0.1 mbar) to remove residual solvent.

The foams were tested for possible solvent residue by headspace gas chromatography. The foams (0.5 g) were dissolved in *N*-methyl-2-pyrrolidone (NMP; 1.5 g) at 50 °C, equilibrated (30 min; 90 °C), and then injected into a headspace gas chromatograph (Headspace sampler HP7694 and Gas Chromatograph 5890 Series II, Hewlet Packard, Palo Alto, USA), where it was heated from 100 to 200 °C. A column (DB 624, J&W Scientific, Folsom, USA) having a flame ionization detector was used for detection.

Morphological investigations

The foam morphology was studied by SEM. The foams were cut in liquid nitrogen, fixed on holders with a conductive adhesive, and sputtered with a 1.5 nm layer of platinum/palladium (Polaron SC7640, Newhaven, Great Britain). The prepared samples were investigated using a LEO 1550 VP electron microscope with a Schottky-Emitter (Zeiss, Jena, Germany) at an acceleration voltage of 3 kV with a maximal resolution of 2.5 nm.

The three-dimensional foam morphology was investigated by µ-CT (Procon X-ray GmbH, Garbsen, Gemany). The sample was irradiated with an x-ray beam. The transmitted intensity was detected by a CCD detector with the absorption being proportional to the density. The material with the higher x-ray absorption generates a shadow picture on the CCD detector. The sample rotates stepwise by 0.45° until a nearly complete rotation of 360°. Transmission light pictures are generated by this procedure. A three-dimensional picture can be reconstructed with the modular constructed software "Mavi" (Fraunhofer Institute of Techno- and Wirtschaftsmathematik, Kaiserslautern, Germany). The three-dimensional shadow pictures are used to determine the pore size distribution and the average pore size including its standard deviation.

The relative content of pores accessible by nitrogen was determined by pycnometry. The measurements were carried out at 20 °C in a 60 cm^3 test cell in an Ultrafoam Pycnometer 1000 (Quantachrome Instruments, Odelzhausen, Germany) using nitrogen as a displacement fluid (6 psi). Each measurement was repeated 10 times and had a maximum standard deviation of 1%. The foam density was calculated from the geometric volume and the mass of the foam sample. The total porosity corresponds to the ratio of the foam volume and the volume of the corresponding compact, non-foamed polymer, which has a density of 1.11 $g \cdot cm^{-3}$.

Determination of the shape-memory properties

Experiments in a thermochamber

The foams were heated in a thermochamber to the programming temperature T_{prog} = 80 °C and were then compressed manually with a compression device to ε_m = 50 % of their original height. They were transferred in the compressed state to a cooling chamber having a temperature of T_{fix} = 5 °C. The compressed foams were placed into a thermochamber having a temperature of 80 °C to investigate the shape-memory effect. The original, the compressed ε_m and restored height ε_p of the foams were measured manually with a vernier caliper.

Experiments with a tensile tester

Shape-memory properties were determined in three subsequent, cyclic, thermomechanical analysis tests on a Zwick Z1.0 compression tester equipped with a

thermochamber (Eurotherm Regler, Limburg, Germany). The samples (3.1 cm in diameter; height of 12 – 17 mm) were compressed at T_{prog} = 80 °C to ε_m = 50% of the original height. Then they were cooled down to T_{fix} = 0 °C to fix the temporary shape ("programming step"). Finally the foam was heated by 2 $K \cdot min^{-1}$ up to 80 °C to investigate the nearly stress-free recovery. The shape-shift was recorded as a function of the temperature for the programming as well as for the shape recovery. The shape-fixity R_f and shape-recovery rates R_r were calculated according to the equations published in [9].

Experiments in an alternating magnetic field

The foams were manually compressed and their shape fixed as described in *2.3.1*. The compressed foams were cut into cylindric specimen with a base area of 44 mm^2 (diameter of 7.5 mm) and cuboid ones with a base area of 12 mm^2. The compressed cylindric or cuboid specimen were placed into the alternating magnetic field at room temperature to investigate the SME. The original, the compressed ε_m and restored height ε_p of the foams were measured manually with a vernier caliper.

The set-up for the investigation in the alternating magnetic field, consisted of a high frequency generator (TIG 5/ 300; Huettinger Electronic, Freiburg, Germany), a water cooled coil with a diameter of 4 cm with 6 loops, and a IR pyrometer (Metis MY84, Sensortherm, Frankfurt, Germany) to measure the surface temperature. The power output of the generator was adjusted to 97% corresponding to a frequency of 255 kHz.

RESULTS AND DISCUSSION

Nanocomposite foams containing magnetic nanoparticles were prepared by TIPS procedure followed by freeze-drying. A cooling procedure was applied, in which the polymer solution containing the nanoparticles (2.5, 5 or 10 wt% nanoparticles) was cooled to 10 °C under stirring and then cooled quickly to – 20 °C. All foams showed a porosity of 93 ± 1%, which was determined gravimetrically, and a quantitative open porosity as determined by pycnometry using nitrogen gas. Alternatively, a slower cooling technique was tried for the foam fabrication as well. However, a strong sedimentation of the brownish-colored nanoparticles, whose color is due to their iron(III) core, to the bottom of the vial was observed and thus this fabrication method was not further persued.

In analogy to foams without nanoparticles[9], the foams showed a bimodal size distribution of large pores with an average diameter of 82±28 µm for C-PEU2.5, which decreased with increasing particle content to 60±27 µm (C-PEU10). Small pores with an average diameter of 10±6 µm (C-PEU2.5) to 9±5 µm (C-PEU5 and C-PEU10) were located within the walls of the large pores. The bimodal size distribution is perceptible in the SEM micrograph (Figure 1a-c). The foams have a brownish color, which is due to the magnetic nanoparticles and intensifies with increasing particle content (Figure 1d).

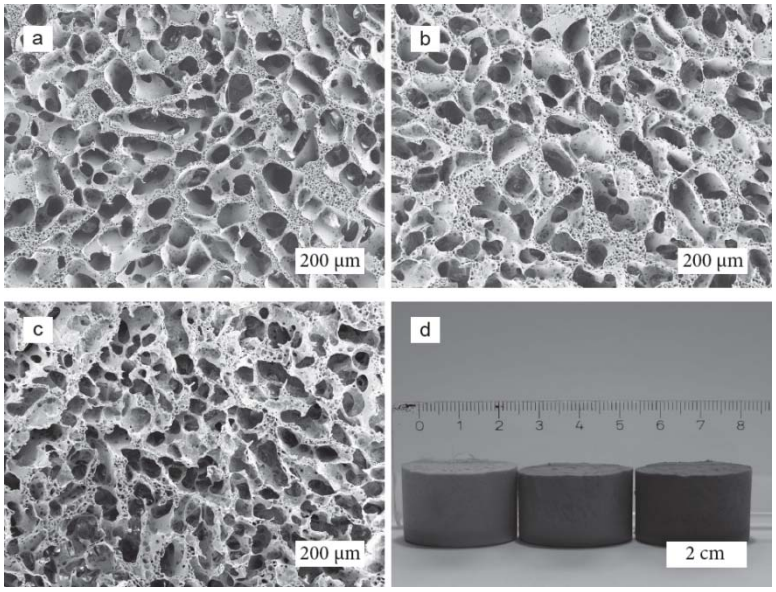

Figure 1: SEM micrographs of the foams (a) C-PEU2.5, (b) C-PEU5, and (c) C-PEU10. A photo shows the foams after removal of the top layer in their original state. Notice the increase in color as particle content increases (from left to right).

Three-dimensional structures of the foams were constructed from µ-CT measurements with a resolution of one voxel, which corresponds to an edge length of 8 µm. The reconstructed morphology is depicted in Figure 2a. Furthermore, µ-CT allows the determination of the pore size distribution and average pore size for all foams (Figure 2 b), although pore sizes below 50 µm are most likely neglected due to the resolution of the instrument. Thus the µCT analysis does not show any increase in relative frequency of the small pores of 5 to 10 µm, which were observed in the SEM micrographs. For C-PEU2.5 an average pore size of 230 µm was determined, the average pore size decreased with higher particle loading to 169 µm for C-PEU5 and to 158 µm for C-PEU10. The higher average pore size of the µ-CT measurement compared to the SEM is accounted to the different evaluation methods. In case of SEM, only the pores as shown in the SEM micrograph are evaluated, thus only a fairly small number is evaluated and the pores of the SEM are not directly cut in the center of each pore, which automatically reduces the determined pore size. The foams with the higher particle loading, i.e. C-PEU5 and C-PEU10, showed a closer pore size distribution than C-PEU2.5 according to µ-CT. The small pores located within the cell walls of the larger pores, as observed in the SEM micrographs, did not lead to an increase of the relative frequency in the size range of 5-15 µm. Because of the resolution limit of the µ-CT analysis, only pore sizes above this size are measured.

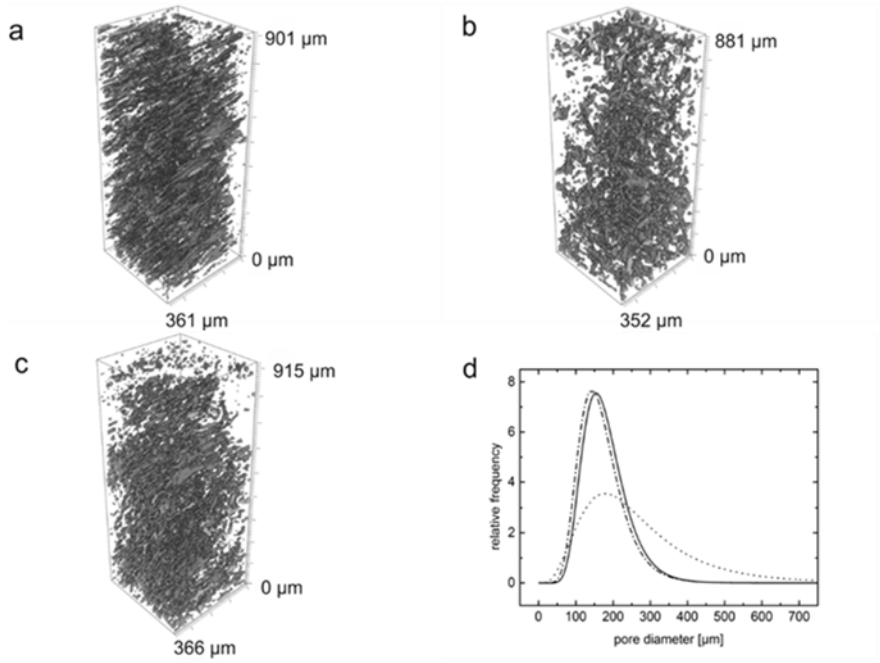

Figure 2: a) Quantitative determination of the pore sizes and pore size distributions based on X-ray micrographs of C-PEU2.5 (dotted), C-PEU5 (line), and C-PEU10 (line-dot). X-ray micrographs show the reconstructed morphology of the foams b) C-PEU2.5, c) C-PEU5, d) C-PEU10.

The SME of the foams was induced in three different settings: thermochamber, tensile tester equipped with a thermochamber and magnetic field. The procedure to quantify the shape-memory properties included for all three methods a programming step in which the foam was compressed to ε_m = 50% of its original height at the programming temperature T_{prog} = 80 °C, followed by a fixation at either T_{fix} = 5 or 0 °C. A SEM of a compressed foam (Figure 3) indicates no breakage of a pore wall during the compression process. After the programming step, the samples were exposed to either environmental heat at T = 80 °C or an alternating magnetic field (30 kAm^{-1}) to initiate the SME. In case of the tensile tester equipped with a thermochamber, this two-step procedure (programming and intiating the SME) was repeated in three consecutive thermomechanical cycles.

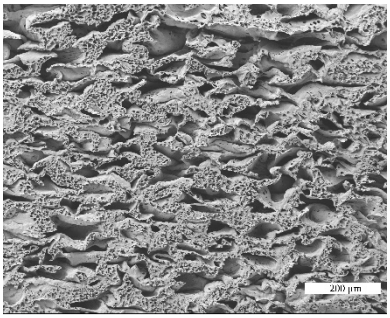

Figure 3: SEM micrograph of a compressed foam

For the testing in a thermochamber, the manually programmed sample was transferred to a thermochamber having T = 80 °C. Under these conditions the foams could recover stress-free and reached recovery rates R_r of around 75% (72 ± 5% for C-PEU2.5, 74 ± 5% for C-PEU5, and 76 ± 4% for C-PEU10) as depicted in Figure 4.

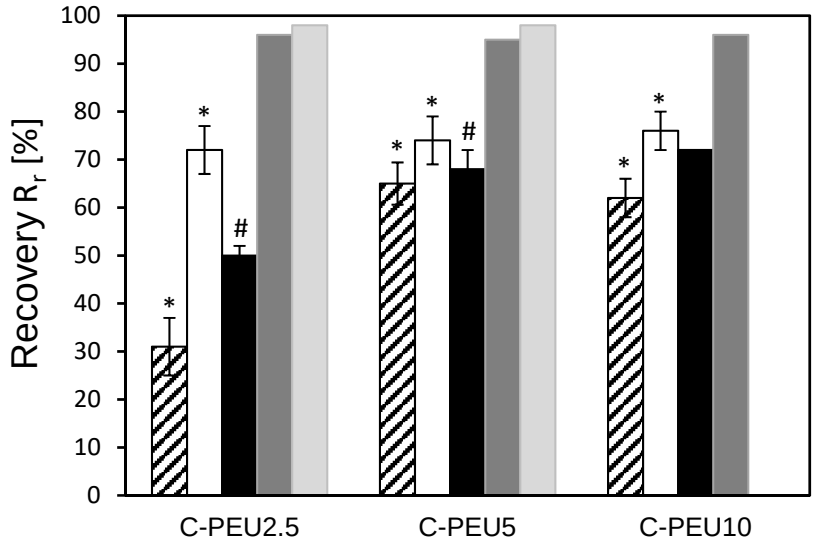

Figure 4: Comparison of R_r of PEU composite foams using different methods of inducing a shape recovery: magnetic field (hatched), thermochamber (white), tensile tester first cycle (black), tensile tester second cycle (dark grey), tensile tester third cycle (light grey). Third cycle was not measured for C-PEU10. Error bars indicate the standard (*) or absolute deviation (#) from the average value. In case of n = 1 no error bar is shown.

The shape-memory properties of the foams were studied in three consecutive thermomechanical cycles in a tensile tester with a thermochamber under stress-free recovery conditions. Figure 5 shows the change in extension and temperature in dependence of time. During the fixation of the temporary shape of the foams a further contraction of the foams by 5 to 6% was observed, which is caused by thermal contraction during cooling and had been observed for the PEU foams without nanoparticles as well [9]. The compression obtained for the temporary shape after removal of load at T_{fix} is

quantitatively described by ε_u. In case of manual programming, no difference was found between ε_U and ε_m resulting in a shape fixity of 100%, which may be due to the inaccuracy of the manual method. The recovery R_r(N=1) for the first cycle increased with increasing amount of nanoparticles from 50 ± 2% (C-PEU2.5) to 68 ± 4% (C-PEU5) and finally to 72% for C-PEU10 (n =1) (Table 1).

Table 1: Shape-memory properties of PEU nanocomposite foams having different contents of magnetic particles determined by tensile tester measurements with N being the number of measurement cycles.

	C-PEU2.5		C-PEU5		C-PEU10	
N	R_r [%]	R_f [%]	R_r [%]	R_f [%]	R_r [%]	R_f [%]
1	50±2	108±0	68±4	108±1	72*	107*
2	96±0	108±0	95*	108*	96*	100*
3	98*	108*	98*	109*	n.d.	107*

*n = 1

Thus, the recovery especially for C-PEU2.5, but also for C-PEU5 is much lower than in the thermochamber. This lower value is expected to be caused by the backpressure of the tensile tester, which is needed by the machine to determine the height of the specimen. In the second and third cycle, the recoveries varied between 95 to 98% independently of the amount of nanoparticles; for C-PEU10 R_r (N = 3) could not be measured because the measurement was disrupted by the machine. This disruption, which was found for several measurements, is accounted to the extremely low back pressure of the tensile tester. The shape fixity ratio for C-PEU2.5 and C-PEU5 was around 108% for all three cycles, while it was slightly lower for C-PEU10 R_f (N = 1) = R_f (N = 3) = 107%, and R_f (N = 2) = 100%. In all cases the switching temperature was 80 °C, which corresponds to the reported switching temperature of the PEU foams without nanoparticles [9]. Compression tests of the foams at room temperature, which revealed a Young's modulus of 1.5±0.5 MPa and a maximum stress of 0.2 MPa, showed no difference between the three foams.

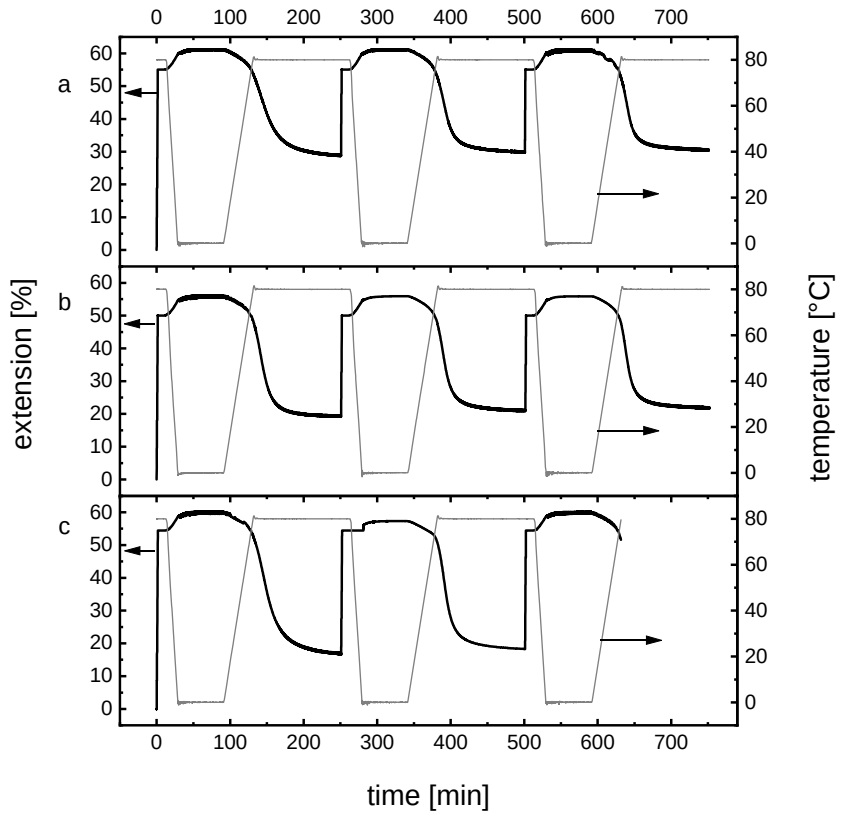

Figure 5: Three consecutive cyclic thermomechanical tests of the nanocomposite foams C-PEU2.5 (a), C-PEU5 (b), C-PEU10 (c) performed in a tensile tester. Each cycle consist of a compression at at 80 °C by 50%, a shape fixation at 0 °C, and a shape-recovery at 80 °C under nearly stress-free conditions.

For determining the shape-memory properties in a magnetic field, the programmed foams were cut into smaller specimen to fit into the magnetic coil of the experimental setup. Special emphasis was put on the selection of the suitable size and geometry of the foams. On the one hand, the maximum dimension of the specimen is limited by the size of the magnetic coil. On the other hand, the foam dimension had to overcome a certain volume to reach the switching temperature in the magnetic field because of the equilibrium of heating by the magnetic field and cooling caused by heat transfer to the environment. Thus two samples of C-PEU10 were tested for shape recovery: cylindrical samples with a base area of 44 mm^2 and a surface (S) to volume (V) ratio of S/V = 0.7, and smaller cuboid ones with a base area of 12 mm^2 and a surface to volume ration of S/V = 1.3. For the calculation of the S/V ratio the surface roughness was not considerated, only the macroscopic dimension of the samples. The exposure to an alternating magnetic field led to an increase of the surface temperature within a few minutes. The cylindrical samples (n= 6) showed higher surface temperature (66 ± 5 °C compared to 46 ± 9 °C of the cuboid ones), which went along with a higher shape recovery

rate (62 ± 5%; standard deviation) than the cuboid samples (n = 4; 46 ± 9%). The lower temperature of the cuboid samples corresponds to the findings reported in [6] for non-porous samples with S/V = 1.4 to 8.1 that the smaller the S/V ratio is, the higher is the achievable temperature. In case of C-PEU2.5 foams, the cylindrical specimen (n = 1) showed a lower surface temperature (30 °C) than the cuboids (32 ± 3 °C; n = 5) which went along with a lower shape recovery (R_r = 24% compared to R_r = 31±7%). Thus in case of C-PEU2.5 the cylindrical geometry showed no benefit, which may be explained by a too low content of magnetic particles to allow a sufficient inductive heating by the applied alternating magnetic field. In case of the C-PEU5 cylindrical foams, a slightly lower surface temperature (63±6 °C) was reached in the magnetic field than for C-PEU10 but the shape recovery ratio was slightly higher (R_r = 65±4%). Generally, a low surface temperature goes along with a low recovery rate. The fact that temperatures as low as 32 °C already lead to a partial shape recovery is explained by the broad glass temperature associated to the switching phase as mentioned earlier. A temperature above 73 °C is required to reach the highest recovery rate.

CONCLUSION

PEU nanocomposite foams prepared by TIPS with different magnetic nanoparticles amounts have been prepared. The particles are well distributed, which is a prerequisite for the homogeneous inductive heating of the composite foam in a magnetic field. SEM micrographs reveal that the foams are open-porous and show a bimodal size distribution with small pores located in the pore walls of the large pores. The foams were tested for their shape recoveries in an alternating magnetic field at room temperature and compared to environmental heating in a thermochamber and in three consecutive thermomechanical cycles in a tensile tester equipped with a thermochamber. The highest recovery rate was achieved in a thermochamber with only marginal differences between the different foams. In the tensile tester lower recovery rates were found in the first cycle than in the thermochamber. A recovery was also achieved by exposure to an alternating magnetic field. In the very best case, the C-PEU5 foams, the recoveries are 9% lower than in the thermochamber. The amount of incorporated magnetic particles had a direct effect on the recovery. 5 wt% loading with magnetic particles was needed to yield a satisfactory shape recovery rate of R_f >65%, while 2.5 wt% loading only reached R_r = 31% because of a too low inductive heating. The lower heating and thus recovery rate in the magnetic field might be overcome by decreasing the environmental cooling of the foam by using closed-porous foams or by covering the present foams with a membrane.

ACKNOWLEDGEMENTS

We thank Regine Apostel for technical assistance in the foam preparation and characterization, Dr. Hans Kosmella for tensile tester measurements and Yvonne Pieper for SEM measurements. This work was financially supported by the Helmholtz-Association through programme-oriented funding and the Ministry for Science, Research and Cultural Affairs of Brandenburg through the grant of the joint project “Konsequenzen der altersassozierten Zell- und Organfunktionen” of the Gesundheitscampus Brandenburg.

REFERENCES

1. H. Meng and G. Q. Li, *Polymer* **54** (9), 2199-2221 (2013).
2. M. C. Serrano and G. A. Ameer, *Macromolecular Bioscience* **12** (9), 1156-1171 (2012).
3. X. Wu, W. M. Huang, Y. Zhao, Z. Ding, C. Tang and J. Zhang, *Polymers* **5** (4), 1169-1202 (2013).
4. V. A. Beloshenko, V. N. Varyukhin and Y. V. Voznyak, *Russian Chemical Reviews* **74** (3), 265-283 (2005).
5. A. Lendlein and O. E. C. Gould, *Nat Rev Mater* **4** (2), 116-133 (2019).
6. R. Mohr, K. Kratz, T. Weigel, M. Lucka-Gabor, M. Moneke and A. Lendlein, *PNAS* **103** (10), 3540-3545 (2006).
7. A. Lendlein and R. Langer, *Science* **296** (5573), 1673-1676 (2002).
8. M. Behl, M. Y. Razzaq and A. Lendlein, *Adv. Mater.* **22** (31), 3388-3410 (2010).
9. T. Sauter, K. Lutzow, M. Schossig, H. Kosmella, T. Weigel, K. Kratz and A. Lendlein, *Adv. Eng. Mater.* **14** (9), 818-824 (2012).
10. S.-Q. Wang, D. Kaneko, M. Okajima, K. Yasaki, S. Tateyama and T. Kaneko, *Angew. Chem. Int. Ed.* **52** (42), 11143-11148 (2013).
11. H. Y. Jiang, S. Kelch and A. Lendlein, *Adv. Mater.* **18** (11), 1471-1475 (2006).
12. D. Habault, H. Zhang and Y. Zhao, *Chemical Society Reviews* **42** (17), 7244-7256 (2013).
13. M. Y. Razzaq, M. Behl and A. Lendlein, *Adv. Funct. Mater.* **22** (1), 184-191 (2012).
14. X. J. Yu, S. B. Zhou, X. T. Zheng, T. Guo, Y. Xiao and B. T. Song, *Nanotechnology* **20** (23) (2009).
15. J. Thevenot, H. Oliveira, O. Sandre and S. Lecommandoux, *Chemical Society Reviews* **42** (17), 7099-7116 (2013).
16. M. Y. Razzaq, M. Behl, K. Kratz and A. Lendlein, *Adv. Mater.* **25** (40), 5730-+ (2013).
17. L. Wang, M. Y. Razzaq, T. Rudolph, M. Heuchel, U. Nochel, U. Mansfeld, Y. Jiang, O. E. C. Gould, M. Behl, K. Kratz and A. Lendlein, *Mater Horiz* **5** (5), 861-867 (2018).
18. T. Weigel, R. Mohr and A. Lendlein, *Smart Mater. Struct.* **18** (2), 025011 (2009).
19. K. Hearon, P. Singhal, J. Horn, W. Small, C. Olsovsky, K. C. Maitland, T. S. Wilson and D. J. Maitland, *Polymer Reviews* **53** (1), 41-75 (2013).
20. A. Metcalfe, A. C. Desfaits, I. Salazkin, L. Yahia, W. M. Sokolowski and J. Raymond, *Biomaterials* **24** (9), 1681-1681 (2003).
21. L. De Nardo, S. Bertoldi, A. Cigada, M. C. Tanzi, H. J. Haugen and S. Fare, *JABFM* **10** (2), 119-126 (2012).
22. H. M. Kim, Z. M. Huang, J. S. Kim, J. R. Youn and Y. S. Song, *Eur. Polym. J.* **106**, 188-195 (2018).
23. J. Y. Wang, J. S. Luo, R. Kunkel, M. Saha, B. N. Bohnstedt, C. H. Lee and Y. T. Liu, *Mater. Lett.* **250**, 38-41 (2019).
24. J. Y. Wang, R. Kunkel, J. S. Luo, Y. H. Li, H. Liu, B. N. Bohnstedt, Y. T. Liu and C. H. Lee, *Polymers* **11** (4), 14 (2019).
25. S. M. Kang, S. J. Lee and B. K. Kim, *Express Polym. Lett.* **6** (1), 63-69 (2012).
26. S. M. Kang, M. J. Kim, S. H. Kwon, H. Park, H. M. Jeong and B. K. Kim, *J. Mater. Sci* **27** (22), 2837-2843 (2012).
27. S. L. Simkevitz and H. E. Naguib, *High Perform. Polym.* **22** (2), 159-183 (2010).
28. H. Kalita and N. Karak, *JNN* **14** (7), 5435-5442 (2014).
29. R. Q. Xie, J. L. Hu, F. Ng, L. Tan, T. W. Qin, M. Q. Zhang and X. Guo, *Ceram. Int.* **43** (6), 4794-4802 (2017).
30. K. Luetzow, F. Klein, T. Weigel, R. Apostel, A. Weiss and A. Lendlein, *J. Biomech.* **40**, S80-S88 (2007).
31. A. S. Rowlands, S. A. Lim, D. Martin and J. J. Cooper-White, *Biomaterials* **28** (12), 2109-2121 (2007).
32. Y. H. Gong, Z. W. Ma, C. Y. Gao, W. Wang and J. C. Shen, *J Appl Polym Sci* **101** (5), 3336-3342 (2006).